I&EC research
Industrial & Engineering Chemistry Research

Article

Cite This: Ind. Eng. Chem. Res. 2018, 57, 139−149

pubs.acs.org/IECR

Examination of Mechanisms for Formation of Volatile Aldehydes from Oxidation of Oil-Based Systems

Lindsay H. Oakley,[†] Francesca Casadio,[§] Kenneth R. Shull,[†] and Linda J. Broadbelt*[,‡]

[†]Department of Materials Science & Engineering and [‡]Department of Chemical & Biological Engineering, Northwestern University, Evanston, Illinois 60208, United States

[§]Department of Conservation, Art Institute of Chicago, 111 South Michigan Avenue, Chicago, Illinois 60603, United States

Supporting Information

ABSTRACT: The mechanisms responsible for the production of small volatile aldehydes during low temperature condensed phase oxidation have been the subject of extensive research, and many pathways have been proposed in the literature. However, many of these mechanisms have yet to be explored quantitatively in the context of a kinetic model. A variety of mechanistic postulates for the formation of the volatile species hexanal, such as direct β-scission of alkoxy radicals, Korcek-like decomposition reactions, intramolecular hydrogen shifts, intramolecular reactions of allylic peroxy species, and scission reactions of higher order oligomeric species, were assembled, and quantum chemical calculations were performed where necessary to obtain estimates of kinetic parameters to test each reaction's kinetic relevance in a microkinetic model for the oxidation of a cobalt-catalyzed ethyl linoleate system. Under atmospheric conditions, scission of chain ends from dimeric species was the largest contributor of hexanal, with an induction time evident. A more detailed experimental data set than previously available in the literature with information in the early (<24 h) time window was obtained by gas chromatography/mass spectrometry headspace analysis, and agreement between the model and the experimental data was vastly improved when the mechanism involving decomposition of dimeric species was included.

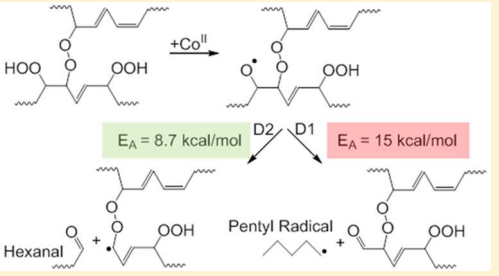

1. INTRODUCTION

The molecules responsible for the characteristic odor of drying oil-based paints or other biobased coatings and products have been captured and identified in several studies, particularly pinpointing the role of small volatile aldehydes.[1−3] While the composition of these volatiles has been established, the mechanisms by which they are produced remain obscured. Understanding these mechanisms is important in multiple contexts. In modern industrial settings, minimizing the production of these volatiles from coated surfaces is desirable to reduce their environmental impact and improve safety.[3−5] In foods containing natural oils, volatile aldehydes sour the taste, and packaging and cooking conditions may need to be optimized to prevent waste.[6−9] Finally, in the context of cultural heritage science for oil paintings and other cultural heritage objects containing oil-based polymers, understanding these mechanisms may lead to crucial insights for preserving and maintaining priceless artworks.[10,11]

Often in cultural heritage science, volatile aldehydes are used as a metric to monitor surfaces for aging, and an increase in the concentration of these molecules is associated with increased degradation.[12] However, this information is chiefly obtained from artificially aged samples where elevated temperature or UV radiation is used to affect observable changes in reasonable time periods in the laboratory. Experimental work has indicated that artificial aging may create samples similar to naturally aged samples in terms of physical properties like brittleness, but may lack the chemical similarity desired for testing cleaning techniques or idealizing environmental conditions using mock-ups.[13,14]

Microkinetic modeling is a powerful tool that can facilitate the exploration of the mechanisms governing the production of these molecules and lead to new mechanistic understanding.[15] This technique is based on elementary steps providing the level of detail required to resolve the mechanistic questions of interest at the molecular level.[16] In previous research, we utilized a microkinetic model to explore the oxidation of an oil paint model system composed of ethyl linoleate and a cobalt catalyst.[17] Available experimental data on the production of volatile molecules from the system included headspace analysis for the period of 100 h, specifically tracking the evolution of hexanal and pentanal with data taken approximately every 24 h.[18] Most of the literature sources explored suggested that the β-scission of a single conjugated alkoxy radical was responsible for the formation of both products, and these routes were included into the microkinetic model for testing.[19−24] However, quantitative comparison of the model results with experimental data confirmed that the route to hexanal was kinetically insignificant. The model predicted that almost no hexanal was

Received: October 7, 2017
Revised: December 4, 2017
Accepted: December 7, 2017
Published: December 7, 2017

Downloaded via NORTHWESTERN UNIV on October 23, 2019 at 03:23:33 (UTC).
See https://pubs.acs.org/sharingguidelines for options on how to legitimately share published articles.

© 2017 American Chemical Society

DOI: 10.1021/acs.iecr.7b04168
Ind. Eng. Chem. Res. 2018, 57, 139−149

formed despite the fact that it is considered a major volatile product, produced in much higher concentrations than pentanal. This is largely due to the fact that a highly unstable vinyl radical is simultaneously created when forming hexanal via β-scission, making the reaction barrier for this elementary step too high to be kinetically relevant at room temperature. This discovery motivated an in depth exploration of alternative mechanisms for the production of hexanal. It should be noted that while this β-scission mechanism may not be the primary pathway for hexanal production at room temperature, it may become important at elevated temperatures used to simulate conditions for artificial aging or other condensed phase, low temperature oxidation scenarios of interest. Thus, additional reaction mechanisms for hexanal formation were sought to add to the model to account for the formation of hexanal at low temperature as well as preserve its ability to account for alternative routes at higher temperatures.

This work examined in detail and tested a number of alternative mechanistic postulates in the context of our previously constructed microkinetic model. Specifically, Korcek and Korcek-like reactions, intramolecular hydrogen shifts followed by subsequent β-scission events, and the cyclization and decomposition of allylic peroxy radicals through a dioxetane intermediate were probed. While these mechanisms have been gleaned from or inspired by chemical mechanisms in the literature, supporting kinetic information was provided in only a few instances. Consequently, we filled in missing kinetic information using quantum chemical calculations. Since many of the intermediate species proposed in these pathways would be extremely difficult to isolate and track with analytical techniques due to their short-lived nature or low concentrations, quantum chemical calculations provide quantitative information about free energy barriers that can be used to compare and assess the kinetic relevance of these alternative mechanisms. Finally, we examined an alternative mechanism not previously proposed in the literature, namely the concerted decomposition of a hydroperoxide and the cobalt-catalyzed decomposition of a dimer formed from the primary products of a conjugated hydroperoxide and a peroxy radical into an alkoxy radical that undergoes a facile β-scission reaction. Each of these mechanisms, their kinetic parameters, and their ability to capture the experimental data are presented below.

The experimental data used to evaluate our model results were derived from two main sources. As previously mentioned, literature data for the reaction conditions of interest exist, but the lack of data in the early curing regime (<24 h), which our model was designed to capture, was problematic. Rather than interpolating the data between 0 and 24 h, we chose to replicate the experiment, with a focus on obtaining data points previously unavailable for these conditions in the early cure regime.

2. COMPUTATIONAL TECHNIQUES

2.1. Quantum Chemical Calculations. As in our previous work, we used simplified molecules for our computational studies to reduce the time and computational resources required for the calculations.[25] Quantum chemical calculations were performed in Gaussian09[26] using the composite method G4.[27] Transition states were identified as first order saddle points with a single imaginary, high amplitude mode. Intrinsic reaction coordinate (IRC) scans were used to confirm that the transition state was connected to the reactants and products of interest. To extract the kinetic quantities of interest, the frequencies for each stationary point were used to determine the temperature-dependent total partition function in the program Calctherm,[28] which could in turn be used to determine the rate constant as a function of temperature via transition state theory.[29] A Wigner tunneling correction was also applied.[30] This allowed the familiar frequency factor, A, and activation energy, E_A, to be extracted from a linear fit of an Arrhenius plot of $\ln(k)$ versus $1/T$. Temperatures ranged from 300−1500 K in 100 K increments.

2.2. Microkinetic Modeling. Microkinetic modeling is a powerful method of exploring key factors that influence the kinetics of reactions on the molecular level and can provide insight into competing mechanisms and potential ways to optimize desired processes. The model was built from elementary reaction steps and requires a detailed knowledge of the chemistry. A list of reaction steps for oxidation including reactions for initiating, propagating and terminating radicals, and associated kinetic parameters and reaction conditions are listed in a previous work.[17] Because a microkinetic model from elementary steps feasible for hydrocarbon oxidation can have on the order of 10^4 unique species, kinetic correlations quantifying the kinetic parameters of reactions of similar chemistry were employed to reduce the number of parameters. In instances where experimental values could not be determined, an Evans−Polanyi correlation was used, which linearly correlated the heat of reaction with the energy of activation: $E_a = E_0 + \alpha\Delta H_R$, where E_0 is the intrinsic activation barrier and α is the transfer coefficient.[31] Values for ΔH_R for a specific reaction can be extracted from experimental literature or calculated using a Benson group additivity method and software available from the *NIST Chemistry WebBook*.[32] Concentration profiles for each species were generated using a kinetic Monte Carlo (KMC) framework based on the classic stochastic simulation algorithm developed by Gillespie.[33−35] Additional mechanistic steps and parameters enumerated in the following sections were added to this foundational KMC model to test for their kinetic relevance for the production of volatile species at room temperature.

3. EXPERIMENTAL DETAILS

3.1. Materials. The reactants, technical grade ethyl linoleate (EL) and Co(II) 2-ethylhexanoate (Co-EH, 65% w/w in mineral spirits), and analytical standards (cyclohexane, hexanal, and pentanal) were purchased from Sigma-Aldrich and used as received.

3.2. GC/MS Headspace Instrumentation and Procedures. The reaction mixture was created by combining 1.014 mL of EL with 0.7 μL of Co-EH catalyst. The time was noted immediately as the initiation of the oxidation reaction. The reaction mixture was then spiked with 92 μL of 0.342 M cyclohexane in xylenes solution as an internal standard. A series of vials, one for each desired time point, was created by placing a 12 μL aliquot of the spiked reaction mixture into each 20 mL vial, which was subsequently closed with an aluminum and Teflon cap and sealed with a crimper. The time between the initiation of the reaction and the analysis of the first time point was approximately 30 min.

Experiments were conducted using an Agilent 7697A Headspace Sampler connected to a 6890 GC system. Vials were allowed to cure in lab atmospheric conditions in a sample tray and at 1 h intervals for the first 20 h; samples were automatically agitated and loaded into a temperature controlled oven at 70 °C. Additional time points were taken at

DOI: 10.1021/acs.iecr.7b04168
Ind. Eng. Chem. Res. 2018, 57, 139−149

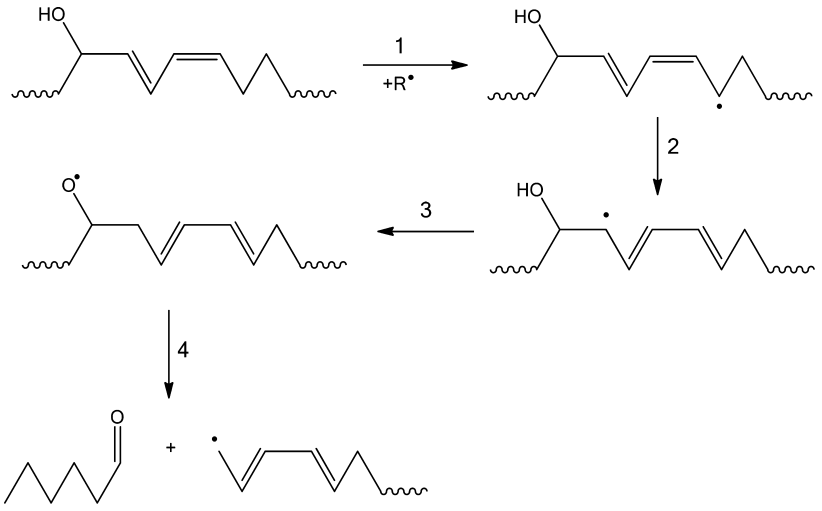

Figure 1. Proposed mechanism for the formation of hexanal and an allylic radical from a series of elementary steps involving (1) hydrogen abstraction from a conjugated alcohol, (2) fast isomerization, (3) an internal hydrogen shift, and (4) the subsequent β-scission of the resulting alkoxy radical.

approximately 30, 50, 70, and 95 h. In the oven, a 100 μL headspace sample was immediately removed by syringe to prevent further sample oxidation and transferred to the gas chromatographer (GC) via a fused silica transfer line held at 115 °C. The syringe was automatically purged for 1 min with helium after the injection was made. Helium was also used as a carrier gas.

The GC system was equipped with a FFAP capillary column (30.0 m long × 250 μm diameter × 0.25 μm film thickness). The GC oven was held initially at 50 °C for 2 min and then ramped up to a maximum temperature of 245 °C at a rate of 20.5 °C/min and held for 8 min. The Quadrapole MS analyzer was operated in electron impact (EI+) ionization mode. Retention times and relative response factors for the compounds of interest were determined from analytical standard references of hexanal, pentanal, and cyclohexane. Integrated peaks from the extracted ion chromatograms for characteristic masses for each compound were used to determine the amounts of volatile compounds produced during the course of the reaction.

4. REACTIONS STUDIED

4.1. Korcek and Korcek-like Reactions. Korcek reactions were originally proposed by Korcek and co-workers in the context of the oxidation of lubricant oils.[36−39] A recent computational study performed by Jalan et al. confirmed some of the main ideas behind the mechanistic propositions of Korcek and co-workers, but with some differences.[40] Using high levels of theory, Jalan and co-workers laid out two separate fragmentation pathways for the formation of aldehydes or ketones and carboxylic acids from keto-hydroperoxides via a cyclic peroxide intermediate. The formation of this cyclic peroxide intermediate could also be strongly catalyzed by the presence of organic acids in the system and can shift the rate-limiting step when a critical concentration threshold was exceeded. Their conclusions highlighted the potential applications for these reactions in many low temperature hydrocarbon oxidation scenarios. The microkinetic model contained mechanisms to produce hydroperoxide and ketone moieties, and thus, the Korcek reaction family was a natural extension of the mechanisms underlying the microkinetic model.

Specifically, elementary steps similar to path A described in their work would produce hexanal if one can imagine extending the C3 keto-peroxide system probed by Jalan et al. to the C20 ethyl linoleate model system. The highest barrier reported for this reaction pathway was 34.7 kcal/mol for the formation of the cyclic peroxide intermediate composed of a five-membered ring. This translates to Arrhenius parameters of $A = 2.1 \times 10^8$ s^{-1} and E_A= 28.0 kcal/mol. Since this barrier was too high to be kinetically relevant at the room temperature conditions of interest, we hypothesized that a less strained, six-membered ring could lower this barrier. Because our system contains a high degree of unsaturation, the effect of unsaturation on the cyclization of a keto-hydroperoxide was also explored for new insights into how this chemistry could be applied in the context of lipid peroxidation. However, analogous pathways for the decomposition of these species with six-membered rings into the expected carbonyl containing products could not be determined using quantum chemical methods.

4.2. Intramolecular Hydrogen Shifts. Intramolecular reactions are another method proposed in the literature related to oxidation of oils and paints for creating hexanal.[41] In the postulated mechanism, a hydrogen is abstracted from an alcohol that is a secondary product. The resulting conjugated radical can then rapidly isomerize to move the double bond in proximity to the alcohol functionality. An intramolecular hydrogen abstraction reaction was then invoked to create an alkoxy radical capable of undergoing β-scission to form hexanal and a terminal allylic radical that is more stable than the vinylic radical produced from the direct β-scission of an alkoxy radical. A schematic of this series of reactions is shown in Figure 1.

To determine the kinetic parameters for this reaction, a combination of existing information in the literature and data from our own quantum chemical calculations was applied. Calculated parameters for the hydrogen abstraction reaction creating the conjugated radical of interest were compared to those derived from existing data in the literature.[42,43] Since these kinetic correlations from the literature were originally developed for short chain saturated hydrocarbons and previous work has demonstrated the importance of thoroughly exploring a range of chemical space when constructing structure−reactivity relationships,[25] we sought to confirm their application

DOI: 10.1021/acs.iecr.7b04168
Ind. Eng. Chem. Res. 2018, 57, 139−149

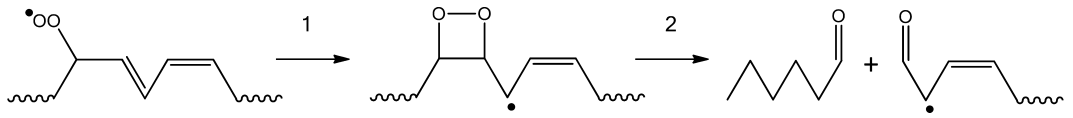

Figure 2. Proposed mechanism forming hexanal through the (1) cyclization of an allylic peroxy radical and (2) subsequent concerted decomposition into two carbonyl-containing species.

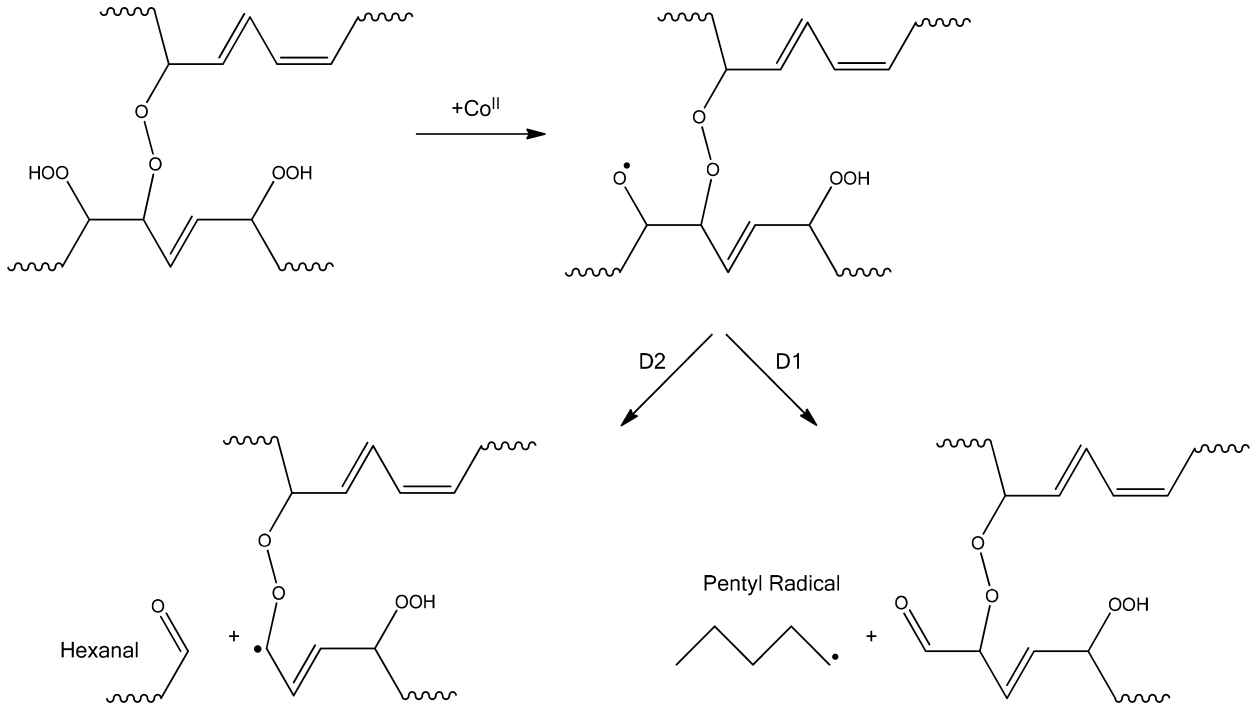

Figure 3. Proposed mechanism for the formation of the small volatile molecules hexanal and pentanal (through the further oxidation of pentyl radicals) from a dimer or higher oligomeric species. Alkoxy radicals are produced by the catalytic activity of cobalt decomposing hydroperoxides, and β-scission can subsequently proceed via pathway D1 or D2.

to systems with increased functionalization and polyunsaturation through our own quantum chemical calculation using the hybrid model chemistry G4 described above on a representative allylic alcohol molecule to ensure accuracy.

4.3. Reactions Involving Allyl Peroxy Species. Many additional mechanisms for the formation of volatile products lay out pathways starting from an allyl peroxy species. These mechanisms all include cyclization steps before decomposition into small molecules. In work by Juita et al., an allyl peroxy radical species, an early species formed by oxygen addition to a conjugated radical, was examined as a major producer of volatiles.[44] Their computational study followed two pathways for the production of small volatile molecules via either a four-membered dioxetane intermediate or a five-membered ring that could decompose in two elementary steps. These pathways are relevant to systems that contain mixtures of fatty acids with multiple points of unsaturation. The desire to produce hexanal from a linoleic acid derivative led us to focus on the formation of volatile products via a four-membered ring. This pathway is reproduced from the work of Juita et al. in Figure 2. Researchers were also unable to locate a transition state along the minimum energy path for the formation of these volatile products from the dioxetane intermediate but estimated the energy barrier to be ~20.1 kcal/mol. This barrier is high to be relevant at room temperature, so additional high level quantum chemical calculations were performed here, using the same G4 method described above, to ensure that no transition states remained unexplored that lead to a lower energy pathway for the production of volatiles at low temperatures.

Because of the demonstrated importance of hydroperoxide species in the kinetic model, a mechanistic pathway starting from a critical conjugated hydroperoxide intermediate was also proposed and investigated using G4. Our postulated mechanism was inspired by Hock cleavage reactions,[45,46] which are typically acid-catalyzed but can occur without the presence of any added acid though a suggested zwitterion geometry by Farmer and Sundralingham.[47,48]

4.4. Formation of Volatile Products from Dimers and Other Higher Order Species. A final mechanism considered for the formation of the volatile product hexanal was inspired by the work of Morita and Tokita.[49,50] Their work proposed and experimentally tested a mechanism for aldehyde formation from the homolytic decomposition of peroxide-linked polymers with hydroperoxide functionalization into hydroxy radicals and aldehydes. This scheme suggested that three bonds would need to be broken, either sequentially or in a concerted fashion, forming four product molecules. This proposed mechanism inspired us to propose our own series of elementary steps involving the decomposition of dimers and other higher order product species to produce volatiles as shown in Figure 3, where a dimer species formed through radical addition and containing hydroperoxide functionalization forms a precursor to an alkoxy β-scission reaction that then forms hexanal and an allylic radical. Our model system of ethyl linoleate assumes the

DOI: 10.1021/acs.iecr.7b04168
Ind. Eng. Chem. Res. 2018, 57, 139−149

presence of cobalt-2-ethyl hexanoate, which catalytically decomposes hydroperoxides into oxygen-centered radicals, thereby facilitating the first step in this pathway. Parameters for the competing reaction that forms pentanal (through the further oxidation of the pentyl radical) were also calculated to assess the relative contribution of this pathway to the quantity of small aldehydes experimentally quantified. The attractive features of the proposed mechanism in Figure 3 are that it is composed of classic free-radical reaction types and that parameters are available from experiment or structure–reactivity relationships.

5. RESULTS AND DISCUSSION

5.1. Experimental Results. Results from the headspace analysis are presented in Figure 4. The experimental error was

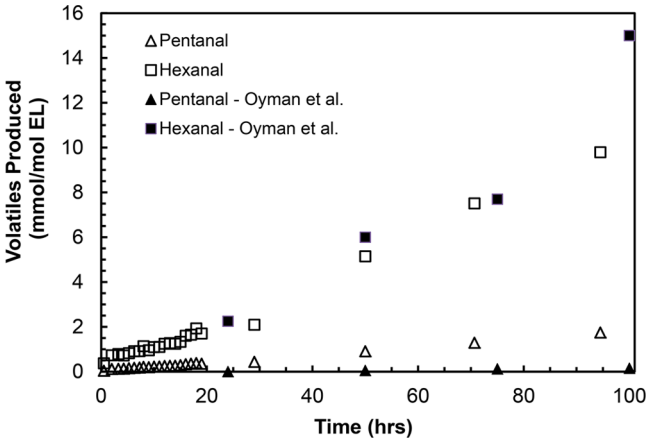

Figure 4. Amount of volatile species hexanal (open squares □) and pentanal (open triangles Δ) detected by GC/MS headspace analysis during the oxidation of EL with a cobalt catalyst. Results are compared to those of Oyman et al.,[18] which are designated using closed symbols.

determined to be approximately 7.5%. The results were compared to the existing literature data from Oyman et al.[18] in the units of mmol per mol of EL, and agreement is generally good for the available data points. New data in the region of 0–20 h again highlighted the expected ratio of the production of hexanal to pentanal, which our earliest kinetic models struggled to capture. Hexanal was initially generated at a rate of about 9.5:1 compared to pentanal and decreased to a ratio of 6:1 as oxidation proceeded. These early curing time points were then used for comparison to kinetic modeling results.

5.2. Computational Results and Implications. A summary of all the mechanisms studied and the associated kinetic parameters is presented in Table 1. The original reactions included in the kinetic model as presented in Figure 6 of ref 17 are labeled as β-scission pathways 1 and 2. Pathway 1 corresponds to the breakdown of a conjugated alkoxy radical into a dienal and an alkyl radical, and pathway 2 leads to the formation of hexanal and the vinyl radical. A sensitivity analysis revealed that the reaction energy barrier of pathway 2 would need to be nearly halved to obtain yields of hexanal and pentanal that would be in reasonable quantitative agreement with experiment assuming that the pre-exponential factor used for the β-scission family remained consistent.

5.2.1. Korcek and Korcek-like Reactions. The results of the quantum chemical calculations are presented in Figure 5 as minimum free energy pathways for the cyclization of representative keto-hydroperoxide species to cyclic peroxides both with and without unsaturation in the final ring. The calculation was designed to mimic the reaction coordinate achieved by Jalan et al. for a slightly larger C4 model keto-peroxide and with the introduction of unsaturated chemical functionality that is integral to lipid oxidation. Overall, the effect of unsaturation on the free energy barrier was mild, only increasing the required energy by ∼1.5 kcal/mol, but some structural observations can be made based on following the reaction coordinate. The lowest energy reactant configuration containing a carbon–carbon double bond is *trans*, but for cyclization to occur, the *cis* isomer must be adopted, which is about 3 kcal/mol higher in energy.

Arrhenius parameters were calculated for both the forward and reverse reactions and are summarized in Table 2. However, as previously mentioned, not much is known about the decomposition of six-membered cyclic peroxide rings, and

Table 1. Summary of Reaction Mechanisms for Production of Small Volatile Aldehydes[a]

mechanism	E_A (kcal/mol)	A (L/mol s or s^{-1})	calculation performed	references and figures
β-Scission, Path 1	11.7	10^{14}	Evans–Polanyi parameters[51] and group additivity[32] to determine ΔH_R	18, 19, 52 Figure 6 of ref 17
β-Scission, Path 2	24.3	10^{14}	Evans–Polanyi parameters[51] and group additivity[32] to determine ΔH_R	19, 53, 54 Figure 6 of ref 17
Korcek Decomposition	28.0	2.1×10^8	Cyclization to a five-membered ring, M06-2X/MG3S	40
	36.7	1.2×10^{11}	Cyclization to a six-membered ring, G4	Figure 5
	38.1	2.4×10^{10}	Cyclization to a six-membered ring with unsaturation, G4	
Intramolecular H-shift	41.5	8.73×10^{11}	G4	41 Figure 1, Figure 6
Concerted Reaction	52.0	6.8×10^{11}	G4	19, 48 Figure 8
Dioxetane Intermediate	24.6	3.9×10^{11}	G4	44, 48 Figure 2, Figure 7
Dimer Decomposition, Path D2	8.7	10^{14}	Evans–Polanyi parameters[51] and group additivity[32] to determine ΔH_R	50 Figure 3, Figure 9

[a]Reaction barriers (E_A) in kcal/mol and pre-exponential factors (A) in L/mol s (bimolecular) or s^{-1} (unimolecular) for rate determining steps are provided, the types of calculations performed to determine these values are indicated and relevant literature describing the mechanism in detail is cited. The number of the relevant figure(s) in the article pertaining to each reaction type is also indicated for ease of reference.

DOI: 10.1021/acs.iecr.7b04168
Ind. Eng. Chem. Res. 2018, 57, 139–149

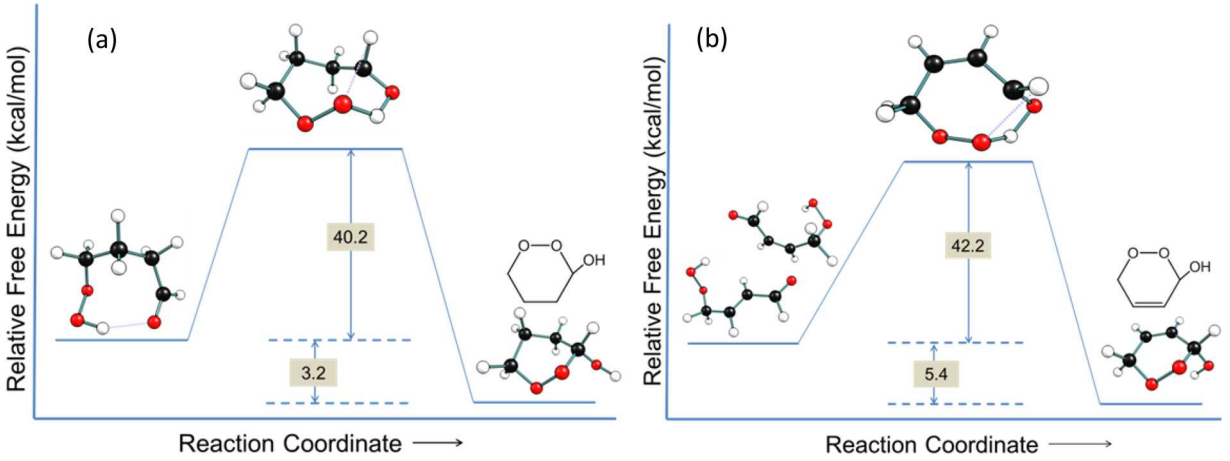

Figure 5. Free energy surfaces for the formation of a six-membered cyclic (a) saturated and (b) unsaturated peroxide species. The unsaturated keto-hydroperoxide must undergo *trans* to *cis* isomerization to obtain the necessary geometry for cyclization to occur.

Table 2. Arrhenius Parameters Calculated for Forward Cyclization and Corresponding Reverse Reactions of Minimum Free Energy Pathways Shown in Figure 5

reaction	A_{fwd} (s^{-1})	$E_{a,fwd}$ (kcal/mol)	A_{rev} (s^{-1})	$E_{a,rev}$ (kcal/mol)
saturated	1.2×10^{11}	36.7	4.1×10^{12}	42.3
unsaturated	2.4×10^{10}	38.1	6.8×10^{12}	46.8

reasonable reaction coordinates for the subsequent fragmentation of these and analogous species to the desired aldehyde products could not be traced using G4.

The high degree of unsaturation present in EL during the early reaction time scale described by our model made placement of a carbonyl group on a carbon γ to a hydroperoxide to create the necessary reactant of Jalan et al. for the formation of a five-membered cyclic peroxide species challenging, and so experimental targets for the production of hexanal could not be met with this mechanism. This observation, however, does not rule out the potential importance of this pathway at longer time scales or at higher temperatures when more of these unsaturated functional groups are consumed. Additionally, for lipid systems without added transition metal catalysts to decompose hydroperoxide moieties, which would compete with Korcek-like reactions, the contribution of this reaction pathway again increases in significance and may particularly influence the formation of organic acids. Further theoretical study of cyclic peroxide fragmentation reactions of larger molecules more representative of unsaturated lipids would play a critical role in determining the responsibility of Korcek decomposition in these types of reaction systems. Deeper mechanistic insights could also be achieved with more quantitative experimental data such as the organic acid concentration profiles for this model EL system.

5.2.2. Intramolecular Hydrogen Shift. The calculated minimum free energy pathway for the 1,3-intramolecular shift of a hydrogen atom of a hydroxyl group is displayed in Figure 6. The geometries of the lowest energy reactant, transition state, and product alkoxy radical are included, which were determined by interrogating all conformational degrees of freedom based on rotations of all dihedral angles. Arrhenius parameters for the forward reaction were calculated to be $A = 8.73 \times 10^{11}$ s^{-1} and E_a= 41.4 kcal/mol. The structure−reactivity relationship presented in the literature for this type of an intramolecular

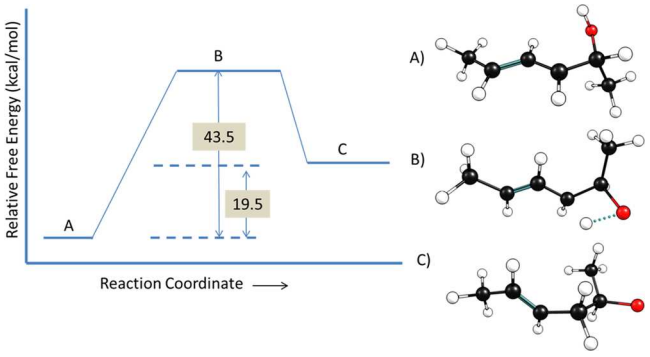

Figure 6. Free energy surface for 1,3-intramolecular hydrogen shift involving a hydroxyl group. Geometries are also shown for the (a) reactant, (b) transition state, and (c) product.

reaction is actually a regression for the energy of activation as a function of TS ring size,[43] as opposed to ΔH_R typical of an Evans−Polanyi relationship, but the concept is similar. When applied to this mechanism, the relationship yielded estimated values of E_a = 41.4 kcal/mol and $A = 3.16 \times 10^{12}$ s^{-1}, which align very closely with the value calculated for this molecule using quantum mechanics.

While this reaction mechanism does ensure that β-scission of the final alkoxy radical product favors the formation of hexanal and an allylic radical, the high ring strain in the four-membered ring transition state rendered this pathway kinetically inconsequential at room temperature.

5.2.3. Reactions with Allylic Peroxy Species. 5.2.3.1. Dioxetane Intermediate. The previous alternatives involving β-scission reaction pathways all proceed through high barriers and thus with small rate constants that cause these mechanisms to be kinetically irrelevant at room temperature. However, rates are a function of both the rate constant and the concentration of the reactant(s), and given the facile formation of peroxy radicals, they were attractive candidates to lead to the formation of aldehydes. Formation of many small molecules directly from a peroxy radical was proposed by Juita et al.[44] Although other volatiles may be formed via lower energy pathways through more stable ring structures, the proposed pathway of interest to form hexanal proceeds through a strained four-membered ring. Given that the researchers were unable to isolate a stable transition state for the decomposition of the dioxetane

DOI: 10.1021/acs.iecr.7b04168
Ind. Eng. Chem. Res. 2018, 57, 139−149

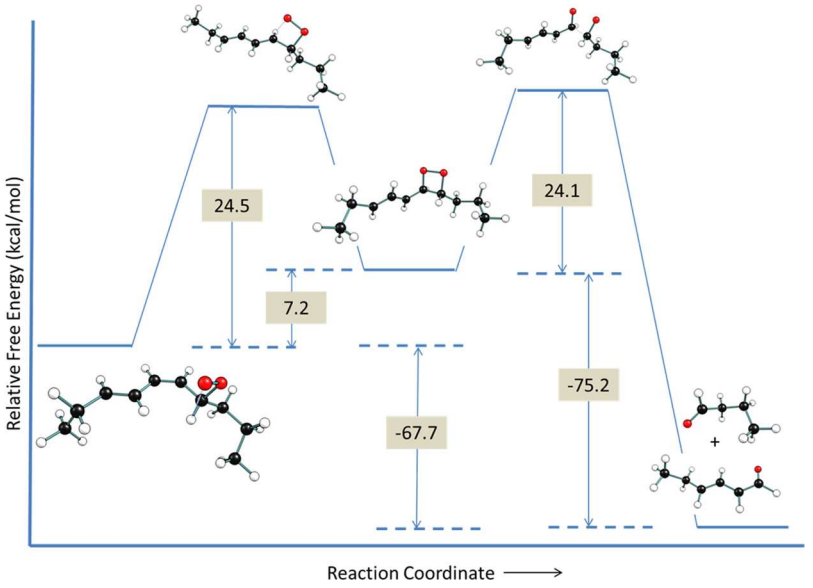

Figure 7. Free energy surface for the formation of two terminal carbonyl species from the decomposition of a peroxy radical. Results are in good agreement with those that Juita et al.[44] were able to report, with the addition of a definitive transition state for the decomposition of the dioxetane intermediate.

intermediate, we sought to confirm the lowest energy pathway for this mechanism with G4 since it has recently been demonstrated to have a high level of chemical accuracy for oxygenated and radical species.[55] As seen in Figure 7, our calculated value for the energy barrier for the first elementary reaction step, cyclization, using the G4 method faithfully reproduced their result of 24 kcal/mol within the expected error for quantum chemical calculations. The Arrhenius parameters subsequently regressed for the forward and reverse reaction steps were determined to be E_a = 24.6 and 18.8 kcal/mol, respectively, with pre-exponential factors of $A = 3.9 \times 10^{11}$ s^{-1} and 4.02×10^{12} s^{-1}.

For the decomposition of this ring, we were able to locate a transition state shown on the potential energy surface in Figure 7. Key structural parameters were a C−C bond length of 1.64 Å and an O−O bond length of 1.87 Å in the fracturing dioxetane ring. Our predicted $\Delta G^{\ddagger}$ was slightly higher than that proposed in the literature. The Arrhenius parameters yielded for this reaction were determined to be E_a = 23.7 kcal/mol and $A = 4.45 \times 10^{12}$ s^{-1}. The associated rate constant was once again too low to be competitive at room temperature for hexanal production as the required peroxy radical reactant readily abstracts abundant biallylic hydrogen atoms from the EL substrate in the early curing regime of interest. However, these reactions were incorporated into the kinetic model to enhance the accuracy of experiments run at a variety of temperatures.

5.2.3.2. Concerted Reaction Pathway. Like the conjugated peroxy radical, an allylic hydroperoxide is a critical reaction intermediate that can build up in the reaction mixture at quite high concentrations until it is catalytically decomposed. Exploring reaction pathways from this species led us to attempt to determine kinetic parameters for a mechanistic postulate proceeding through a zwitterion as originally proposed by Farmer and Sundralingham.[47] While it was not possible to stabilize a zwitterion, the exploration did lead to the discovery of a concerted decomposition reaction. The transition state geometry of this intramolecular reaction is shown in Figure 8. Key parameters for the breaking bonds were O−O = 1.80 Å

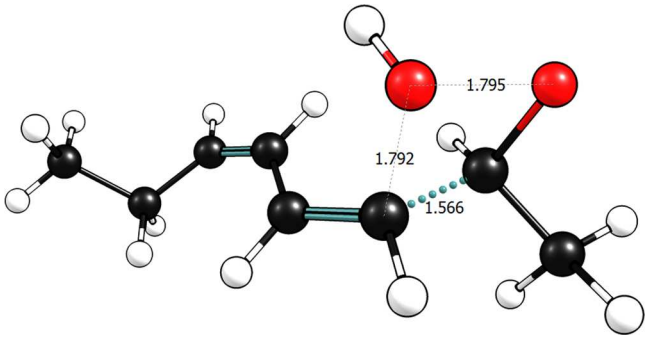

Figure 8. Structure of the transition state for the concerted decomposition of a conjugated hydroperoxide into an aldehyde and an alcohol. Relevant interatomic distances are included in Angstroms (Å).

and C−C = 1.57 Å, and the forming bond between the oxygen of the transferring hydroxyl group and the sp^2 carbon was 1.80 Å at the transition state.

While the activation energy for this reaction, E_a= 52.0 kcal/mol, and the pre-exponential factor, $A = 6.8 \times 10^{11}$ s^{-1}, resulted in a calculated rate constant that excluded this reaction as a possible candidate for hexanal formation, it offers a new pathway for the formation of volatiles during hydrocarbon oxidation at much higher reaction temperatures that could be relevant to, for example, oil oxidation in food applications.[56]

5.2.4. Formation of Volatile Products from Dimers and Other Higher Order Species. Our final mechanistic postulate was inspired by the work of Morita et al.[50] In their work, they offered a key insight that small volatiles may actually be primarily produced from larger secondary products rather than from reactants or primary products. Previous mechanistic alternatives to β-scission pathway 2 (Table 1) all required routes that involved high energy barriers as conjugated double bonds were reoriented into a position convenient for hexanal formation. However, in this mechanistic postulate, the presence of the conjugated double bonds was exploited as shown in Figure 9 to create a dimeric species with a low energy barrier to

DOI: 10.1021/acs.iecr.7b04168
Ind. Eng. Chem. Res. 2018, 57, 139−149

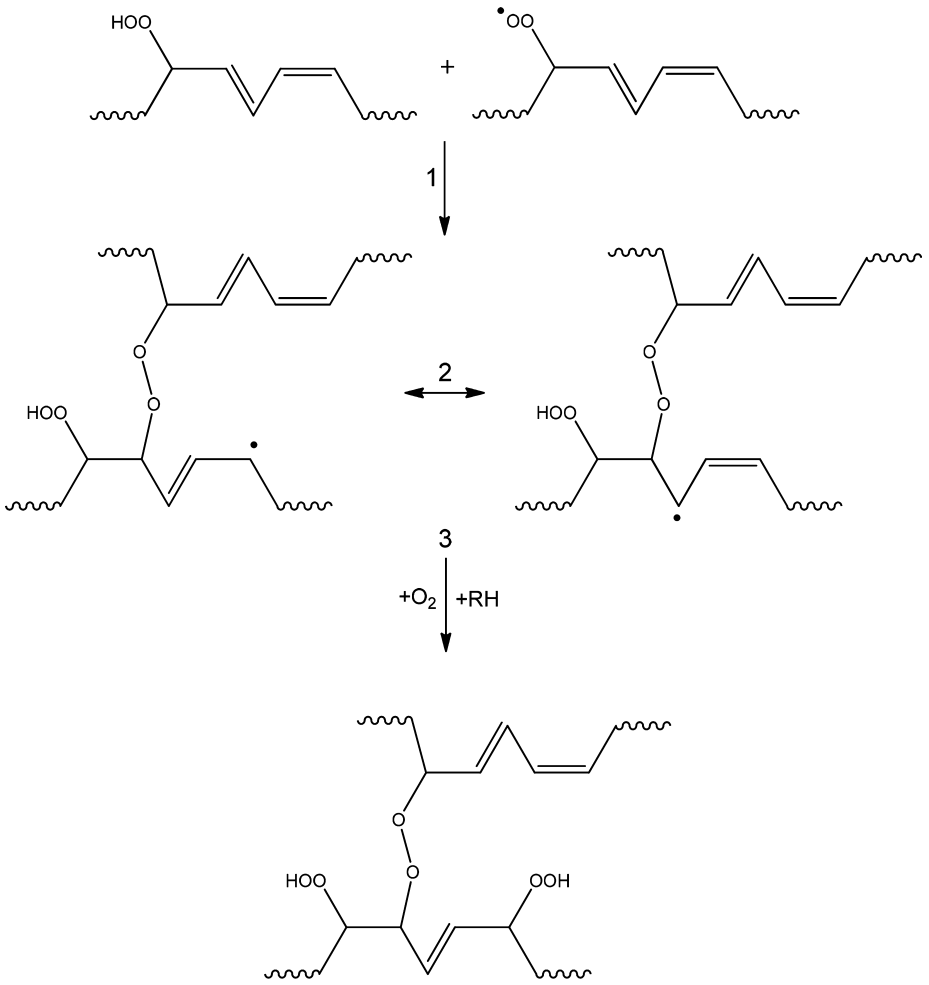

Figure 9. Scheme for the formation of a dimeric species through (1) peroxy radical addition across conjugated double bonds followed by the (2) potential isomerization of the allylic radical and (3) oxygen addition and hydrogen abstraction to form the second hydroperoxide group.

forming hexanal through traditional alkoxy β-scission (Figure 3, Path D2).

Radical addition reactions by peroxy radicals across conjugated double bonds are highly exothermic and facile. Using Evans–Polanyi parameters[16] and heats of reaction calculated using Benson group additivity values,[32] the energy of activation for radical addition to form a dimeric species is 6.7 kcal/mol. In addition, a typical frequency factor for this reaction family is $A = 1 \times 10^8$ M^{-1} s^{-1}. Once this radical species is formed, oxygen addition is rapid. Another hydrogen abstraction reaction forms the dihydroperoxide dimeric species depicted in Figure 3 and Figure 9.

Next, the kinetic model included routes for hydroperoxide functionalities to be catalytically decomposed by the presence of cobalt metal ions into peroxy and alkoxy radicals. The alkoxy radical resulting from this catalytic decomposition could then undergo β-scission (pathway D2), leading to hexanal via a much lower barrier of 8.7 kcal/mol compared to pathway 2 (Table 1). When each of these reactions and kinetic parameters was incorporated into the kinetic model, the result was a significant increase in hexanal production and a decrease in overall pentanal production as shown in Figure 10 relative to our previous results.[17]

These mechanisms imply an induction time for the formation of hexanal relative to pentanal, although it was ultimately a major product formed in much higher quantities than pentanal

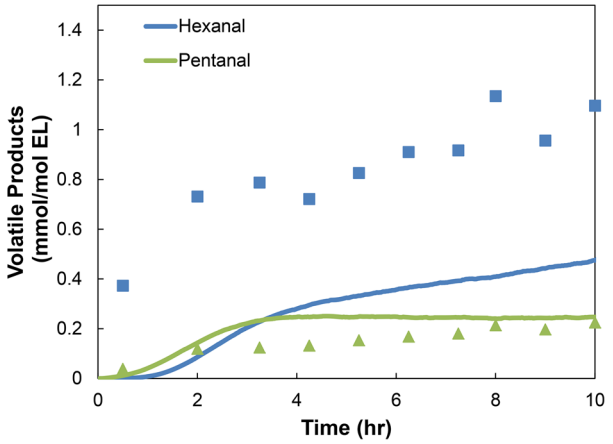

Figure 10. Concentration profiles for the volatile aldehydes, hexanal and pentanal, generated by the microkinetic model (lines). Agreement with measured experimental values (hexanal ■, pentanal ▲) is vastly improved from previous versions of the model that did not allow for volatiles to be formed from higher rank products.

at these temperatures. This new mechanism offers promising pathways for the formation of these species at room temperature. Given the fast curing rate of EL, and other metal catalyzed oil-based systems, several data points within the first 24 h of curing time were needed to develop a thorough

DOI: 10.1021/acs.iecr.7b04168
Ind. Eng. Chem. Res. 2018, 57, 139–149

mechanistic understanding of the formation of volatile species, a gap we sought to fill with the experimental data presented in this work. Data at these lower temperatures offer valuable quantitative targets for comparison during the iterative process of model development and optimization.

A comparison of the theoretical prediction of the model to experiment indicates that the further oxidation of pentyl radicals produced from β-Scission pathway 1, as described in Table 1, was indeed the main source of volatile pentanal. The model still underestimates the experimental predictions of hexanal relative to experiment, but this could be due to the stoichiometric limits placed on the model by restricting the model size to only include monomeric and dimeric species as well as constraining the peroxy radicals allowed to undergo radical addition to the two major conjugated radical C20 isomers found in the system. Theoretically, the identity of the peroxy radical that adds to the double bond needs not be so limited and any higher rank oligomer with the appropriate alkoxy radical β to a peroxy bond should be able to form hexanal from the chain end scission.

Ultimately, this mechanistic proposal for the formation of hexanal did not involve new reaction families, but rather a specific sequence of elementary steps derived from known reaction families, building on many years of detailed research in the field of hydrocarbon oxidation. We do acknowledge, however, that the combinations of possible reactions explored here may not be exhaustive. One can imagine that with a larger reaction network generated automatically to even higher rank products, other kinetically significant pathways may emerge. This endeavor is currently underway.

6. CONCLUSIONS

Through the use of computational approaches, this work explored numerous mechanisms for the formation of volatile products, focusing on hexanal in particular. In the context of a microkinetic model, mechanistic postulates parametrized by theory or structure−property relationships such as the Evans−Polanyi relationship were tested for their kinetic relevance within the range of expected computational error. Most of the pathways tested in this work were appropriate for oxidation chemistry performed at conditions more extreme than room temperature. Our results indicated that a reasonable mechanism for the formation of volatile products at room temperature could be accomplished by the scission of chain ends from higher order (dimeric or larger oligomeric) species. This conclusion was tested through the comparison of newly obtained experimental data from GC/MS headspace analysis in the early cure regime.

This mechanism also has important implications for the formation of an overall cured coating. If elevated temperatures shift the competition between intermolecular addition and abstraction reactions that propagate chain growth to favor intramolecular reactions that lead to chain scission, artificially aged mock-ups of paint layers will not demonstrate the same level of stability as their naturally aged counterparts, making treatment decisions for art objects based on the response of samples aged in this way less meaningful. Computational models have the ability to readily explore the effects of a variety of environmental conditions and could be used to quickly optimize artificial aging parameters. With newly acquired headspace data in the early cure regime now available to calibrate model parameters, the benefits of constructing detailed models of chemical pathways to develop a fundamental understanding of oil-based materials' evolution in time as demonstrated here could extend to other systems involving oxidation chemistry.

■ ASSOCIATED CONTENT

Supporting Information

The Supporting Information is available free of charge on the ACS Publications website at DOI: 10.1021/acs.iecr.7b04168.

Complete library of species and coordinate geometries for each quantum chemical calculation performed (PDF)

■ AUTHOR INFORMATION

Corresponding Author

*E-mail: broadbelt@northwestern.edu. Phone: (847) 467-1751. Fax: (847) 491-3728.

ORCID

Kenneth R. Shull: 0000-0002-8027-900X

Linda J. Broadbelt: 0000-0003-4253-592X

Notes

The authors declare no competing financial interest.

■ ACKNOWLEDGMENTS

Financial support for this work from the National Science Foundation Division of Materials Research (DMR-1241667) and the Northwestern University/Art Institute of Chicago Center for Scientific Studies in the Arts (NU-ACCESS) is gratefully acknowledged. This work used the Extreme Science and Engineering Discovery Environment (XSEDE), which is supported by National Science Foundation grant number ACI-1053575. GC/MS headspace analysis experiments were performed at the Northwestern Integrated Molecular Structure and Education Research Center (IMSERC), which has received support from the Soft and Hybrid Nanotechnology Experimental (SHyNE) Resource (NSF NNCI-1542205), the State of Illinois, and International Institute for Nanotechnology (IIN). Helpful conversations with Dr. Ken Sutherland (AIC) and Director of IMSERC Mass Spectrometry, Dr. S. Habibi Goudarzi, are also gratefully acknowledged.

■ REFERENCES

(1) Fjällström, P.; Andersson, B.; Nilsson, C.; Andersson, K. Drying of Linseed Oil Paints: A Laboratory Study of Aldehyde Emissions. *Ind. Crops Prod.* **2002**, *16* (3), 173−184.

(2) Knudsen, H. N.; Clausen, P. A.; Wilkins, C. K.; Wolkoff, P. Sensory and Chemical Evaluation of Odorous Emissions from Building Products with and without Linseed Oil. *Build. Environ.* **2007**, *42* (12), 4059−4067.

(3) Clausen, P. A.; Knudsen, H. N.; Larsen, K.; Kofoed-Sørensen, V.; Wolkoff, P.; Wilkins, C. K. Use of Thermal Desorption Gas Chromatography−Olfactometry/Mass Spectrometry for the Comparison of Identified and Unidentified Odor Active Compounds Emitted from Building Products Containing Linseed Oil. *J. Chromatogr. A* **2008**, *1210* (2), 203−211.

(4) Haghighat, F.; De Bellis, L. Material Emission Rates: Literature Review, and the Impact of Indoor Air Temperature and Relative Humidity. *Build. Environ.* **1998**, *33* (5), 261−277.

(5) Uhde, E.; Salthammer, T. Impact of Reaction Products from Building Materials and Furnishings on Indoor Air Quality—A Review of Recent Advances in Indoor Chemistry. *Atmos. Environ.* **2007**, *41* (15), 3111−3128.

(6) Jiménez, A.; Beltrán, G.; Aguilera, M. P. Application of Solid-Phase Microextraction to the Analysis of Volatile Compounds in Virgin Olive Oils. *J. Chromatogr. A* **2004**, *1028* (2), 321−324.

(7) Muik, B.; Lendl, B.; Molina-Díaz, A.; Ayora-Cañada, M. J. Direct Monitoring of Lipid Oxidation in Edible Oils by Fourier Transform Raman Spectroscopy. *Chem. Phys. Lipids* **2005**, *134* (2), 173−182.
(8) Krist, S.; Stuebiger, G.; Unterweger, H.; Bandion, F.; Buchbauer, G. Analysis of Volatile Compounds and Triglycerides of Seed Oils Extracted from Different Poppy Varieties (Papaver Somniferum L.). *J. Agric. Food Chem.* **2005**, *53* (21), 8310−8316.
(9) Krist, S.; Stuebiger, G.; Bail, S.; Unterweger, H. Analysis of Volatile Compounds and Triacylglycerol Composition of Fatty Seed Oil Gained from Flax and False Flax. *Eur. J. Lipid Sci. Technol.* **2006**, *108* (1), 48−60.
(10) Lattuati-Derieux, A.; Thao, S.; Langlois, J.; Regert, M. First Results on Headspace-Solid Phase Microextraction-Gas Chromatography/Mass Spectrometry of Volatile Organic Compounds Emitted by Wax Objects in Museums. *J. Chromatogr. A* **2008**, *1187* (1−2), 239−249.
(11) Curran, K.; Underhill, M.; Gibson, L. T.; Strlic, M. The Development of a SPME-GC/MS Method for the Analysis of VOC Emissions from Historic Plastic and Rubber Materials. *Microchem. J.* **2016**, *124*, 909−918.
(12) Curran, K.; Strlič, M. Polymers and Volatiles: Using VOC Analysis for the Conservation of Plastic and Rubber Objects. *Stud. Conserv.* **2015**, *60* (1), 1−14.
(13) Erhardt, D.; Tumosa, C. S.; Mecklenburg, M. F. Natural and Accelerated Thermal Aging of Oil Paint Films. In *Tradition and Innovation, Advances in Conservation*; IIC: Melbourne, 2000; pp 65−69.
(14) Erhardt, D.; Tumosa, C. S.; Mecklenburg, M. F. Long Term Chemical and Physical Processes in Oil Paint Films. *Stud. Conserv.* **2005**, *50* (2), 143−150.
(15) Vinu, R.; Levine, S. E.; Wang, L.; Broadbelt, L. J. Detailed Mechanistic Modeling of Poly (Styrene Peroxide) Pyrolysis Using Kinetic Monte Carlo Simulation. *Chem. Eng. Sci.* **2012**, *69* (1), 456−471.
(16) Vinu, R.; Broadbelt, L. J. Unraveling Reaction Pathways and Specifying Reaction Kinetics for Complex Systems. *Annu. Rev. Chem. Biomol. Eng.* **2012**, *3*, 29−54.
(17) Oakley, L.; Casadio, F.; Shull, K.; Broadbelt, L. Microkinetic Modeling of the Autoxidative Curing of an Alkyd and Oil-Based Paint Model System. *Appl. Phys. A: Mater. Sci. Process.* **2015**, *121*, 869−878.
(18) Oyman, Z. O.; Ming, W.; van der Linde, R.; van Gorkum, R.; Bouwman, E. Effect of [Mn(acac)3] and Its Combination with 2,2-Bipyridine on the Autoxidation and Oligomerisation of Ethyl Linoleate. *Polymer* **2005**, *46* (6), 1731−1738.
(19) Frankel, E. N. Volatile Lipid Oxidation Products. *Prog. Lipid Res.* **1983**, *22* (1), 1−33.
(20) Frankel, E. N. *Lipid Oxidation*; Woodhead Publishing: Cambridge, 2012.
(21) Gardner, H. W.; Selke, E. Volatiles from Thermal Decomposition of Isomeric Methyl (12S, 13S)-(E)-12, 13-Epoxy-9-Hydroperoxy-10-Octadecenoates. *Lipids* **1984**, *19* (6), 375−380.
(22) Muizebelt, W. J.; Donkerbroek, J. J.; Nielen, M. W. F.; Hussem, J. B.; Biemond, M. E. F.; Klaasen, R. P.; Zabel, K. H. Oxidative Crosslinking of Alkyd Resins Studied with Mass Spectrometry and NMR Using Model Compounds. *J. Coat. Technol.* **1998**, *70* (876), 83−93.
(23) Lazzari, M.; Chiantore, O. Drying and Oxidative Degradation of Linseed Oil. *Polym. Degrad. Stab.* **1999**, *65* (2), 303−313.
(24) Soucek, M. D.; Khattab, T.; Wu, J. Review of Autoxidation and Driers. *Prog. Org. Coat.* **2012**, *73* (4), 435−454.
(25) Oakley, L. H.; Casadio, F.; Shull, K. R.; Broadbelt, L. J. Theoretical Study of Epoxidation Reactions Relevant to Hydrocarbon Oxidation. *Ind. Eng. Chem. Res.* **2017**, *56* (26), 7454−7461.
(26) Frisch, M. J.; Trucks, G. W.; Schlegel, H. B.; Scuseria, G. E.; Robb, M. A.; Cheeseman, J. R.; Scalmani, G.; Barone, V.; Mennucci, B.; Petersson, G. A.; Nakatsuji, H.; Caricato, M.; Li, X.; Hratchian, H. P.; Izmaylov, A. F.; Bloino, J.; Zheng, G.; Sonnenberg, J. L.; Hada, M.; Ehara, M.; Toyota, K.; Fukuda, R.; Hasegawa, J.; Ishida, M.; Nakajima, T.; Honda, Y.; Kitao, O.; Nakai, H.; Vreven, T.; Montgomery, J. A., Jr.; Peralta, J. E.; Ogliaro, F.; Bearpark, M.; Heyd, J. J.; Brothers, E.; Kudin, K. N.; Staroverov, V. N.; Kobayashi, R.; Normand, J.; Raghavachari, K.; Rendell, A.; Burant, J. C.; Iyengar, S. S.; Tomasi, J.; Cossi, M.; Rega, N.; Millam, J. M.; Klene, M.; Knox, J. E.; Cross, J. B.; Bakken, V.; Adamo, C.; Jaramillo, J.; Gomperts, R.; Stratmann, R. E.; Yazyev, O.; Austin, A. J.; Cammi, R.; Pomelli, C.; Ochterski, J. W.; Martin, R. L.; Morokuma, K.; Zakrzewski, V. G.; Voth, G. A.; Salvador, P.; Dannenberg, J. J.; Dapprich, S.; Daniels, A. D.; Farkas, O.; Foresman, J. B.; Ortiz, J. V.; Cioslowski, J.; Fox, D. J. *Gaussian 09*; Gaussian, Inc.: Wallingford, CT, 2009.
(27) Curtiss, L. A.; Redfern, P. C.; Raghavachari, K. Gaussian-4 Theory. *J. Chem. Phys.* **2007**, *126* (8), 084108.
(28) Pfaendtner, J.; Yu, X.; Broadbelt, L. J. The 1-D Hindered Rotor Approximation. *Theor. Chem. Acc.* **2007**, *118* (5−6), 881−898.
(29) Moore, J. W.; Pearson, R. G. *Kinetics and Mechanism*, 3rd ed.; John Wiley & Sons: New York, 1981.
(30) Hirschfelder, J. O.; Wigner, E. Some Quantum Mechanical Considerations in the Theory of Reactions Involving an Activation Energy. *J. Chem. Phys.* **1939**, *7*, 616−628.
(31) Evans, M. G.; Polanyi, M. Inertia and Driving Force of Chemical Reactions. *Trans. Faraday Soc.* **1938**, *34*, 11−24.
(32) Stein, S. E.; Rukkers, J. M.; Brown, R. L. *NIST Standard Reference Database 25: NIST Structures and Properties Database and Estimation Program*; NIST: Gaithersberg, MD, 1991.
(33) Gillespie, D. T. A General Method for Numerically Simulating the Stochastic Time Evolution of Coupled Chemical Reactions. *J. Comput. Phys.* **1976**, *22*, 403−434.
(34) Gillespie, D. T. Concerning the Validity of the Stochastic Approach to Chemical Kinetics. *J. Stat. Phys.* **1977**, *16*, 311−318.
(35) Gillespie, D. T. Stochastic Simulation of Chemical Kinetics. *Annu. Rev. Phys. Chem.* **2007**, *58* (1), 35−55.
(36) Jensen, R. K.; Korcek, S.; Mahoney, L. R.; Zinbo, M. Liquid-Phase Autoxidation of Organic Compounds at Elevated Temperatures. 1. The Stirred Flow Reactor Technique and Analysis of Primary Products from N-Hexadecane Autoxidation at 120−180. Degree. C. *J. Am. Chem. Soc.* **1979**, *101* (25), 7574−7584.
(37) Jensen, R. K.; Korcek, S.; Mahoney, L. R.; Zinbo, M. Liquid-Phase Autoxidation of Organic Compounds at Elevated Temperatures. 2. Kinetics and Mechanisms of the Formation of Cleavage Products in N-Hexadecane Autoxidation. *J. Am. Chem. Soc.* **1981**, *103* (7), 1742−1749.
(38) Jensen, R. K.; Korcek, S.; Zinbo, M.; Johnson, M. D. Initiation in Hydrocarbon Autoxidation at Elevated Temperatures. *Int. J. Chem. Kinet.* **1990**, *22* (10), 1095−1107.
(39) Hamilton, E. J.; Korcek, S.; Mahoney, L. R.; Zinbo, M. Kinetics and Mechanism of the Autoxidation of Pentaerythrityl Tetraheptanoate at 180−220 °C. *Int. J. Chem. Kinet.* **1980**, *12* (9), 577−603.
(40) Jalan, A.; Alecu, I. M.; Meana-Pañeda, R.; Aguilera-Iparraguirre, J.; Yang, K. R.; Merchant, S. S.; Truhlar, D. G.; Green, W. H. New Pathways for Formation of Acids and Carbonyl Products in Low-Temperature Oxidation: The Korcek Decomposition of γ-Ketohydroperoxides. *J. Am. Chem. Soc.* **2013**, *135* (30), 11100−11114.
(41) Scalarone, D.; Lazzari, M.; Chiantore, O. Thermally Assisted Hydrolysis and Methylation-Pyrolysis-Gas Chromatography/Mass Spectrometry of Light-Aged Linseed Oil. *J. Anal. Appl. Pyrolysis* **2001**, *58-59*, 503−512.
(42) *Standard Reference Database 17*; NIST, 2015.
(43) Pfaendtner, J.; Yu, X.; Broadbelt, L. J. Quantum Chemical Investigation of Low-Temperature Intramolecular Hydrogen Transfer Reactions of Hydrocarbons. *J. Phys. Chem. A* **2006**, *110* (37), 10863−10871.
(44) Juita; Dlugogorski, B. Z.; Kennedy, E. M.; Mackie, J. C. Mechanism of Formation of Volatile Organic Compounds from Oxidation of Linseed Oil. *Ind. Eng. Chem. Res.* **2012**, *51* (16), 5653−5661.
(45) Schneider, C.; Boeglin, W. E.; Yin, H.; Stec, D. F.; Hachey, D. L.; Porter, N. A.; Brash, A. R. Synthesis of Dihydroperoxides of Linoleic and Linolenic Acids and Studies on Their Transformation to 4-Hydroperoxynonenal. *Lipids* **2005**, *40* (11), 1155−1162.

DOI: 10.1021/acs.iecr.7b04168
Ind. Eng. Chem. Res. 2018, 57, 139−149

(46) Spickett, C. M. The Lipid Peroxidation Product 4-Hydroxy-2-Nonenal: Advances in Chemistry and Analysis. *Redox Biol.* **2013**, *1* (1), 145−152.
(47) Farmer, E. H.; Bloomfield, G. F.; Sundralingam, A.; Sutton, D. A. The Course and Mechanism of Autoxidation Reactions in Olefinic and Polyolefinic Substances, Including Rubber. *Trans. Faraday Soc.* **1942**, *38*, 348−356.
(48) Frimer, A. A. The Reaction of Singlet Oxygen with Olefins: The Question of Mechanism. *Chem. Rev.* **1979**, *79* (5), 359−387.
(49) Morita, M.; Tokita, M. The Real Radical Generator Other than Main-Product Hydroperoxide in Lipid Autoxidation. *Lipids* **2006**, *41* (1), 91−95.
(50) Morita, M.; Tokita, M. Hydroxy Radical, Hexanal, and Decadienal Generation by Autocatalysts in Autoxidation of Linoleate Alone and with Eleostearate. *Lipids* **2008**, *43* (7), 589−597.
(51) Pfaendtner, J.; Broadbelt, L. J. Mechanistic Modeling of Lubricant Degradation. 1. Structure-Reactivity Relationships for Free-Radical Oxidation. *Ind. Eng. Chem. Res.* **2008**, *47* (9), 2886−2896.
(52) Hancock, R. A.; Leeves, N. J.; Nicks, P. F. Studies in Autoxidation: Part I. The Volatile By-Products Resulting from the Autoxidation of Unsaturated Fatty Acid Methyl Esters. *Prog. Org. Coat.* **1989**, *17* (3), 321−336.
(53) Evans, C. D.; List, G. R.; Dolev, A.; McConnell, D. G.; Hoffmann, R. L. Pentane from Thermal Decomposition of Lipoxidase-Derived Products. *Lipids* **1967**, *2* (5), 432−434.
(54) Jeleń, H. H.; Obuchowska, M.; Zawirska-Wojtasiak, R.; Wąsowicz, E. Headspace Solid-Phase Microextraction Use for the Characterization of Volatile Compounds in Vegetable Oils of Different Sensory Quality. *J. Agric. Food Chem.* **2000**, *48* (6), 2360−2367.
(55) Somers, K. P.; Simmie, J. M. Benchmarking Compound Methods (CBS-QB3, CBS-APNO, G3, G4, W1BD) against the Active Thermochemical Tables: Formation Enthalpies of Radicals. *J. Phys. Chem. A* **2015**, *119* (33), 8922−8933.
(56) Dobarganes, M. C.; Marquez-Ruiz, G. Formation and Analysis of Oxidized Monomeric, Dimeric and Higher Oligomeric Triglycerides. *Deep Frying: Chemistry, Nutrition and Practical Applications* **2007**, 87−110.

DOI: 10.1021/acs.iecr.7b04168
Ind. Eng. Chem. Res. 2018, 57, 139−149